Defibrillation Thresholds: A Generalised Polynomial Chaos Study

Peter R Johnston

Griffith University
Brisbane, Queensland, Australia

Abstract

This study aims to understand the effect of variations in cardiac conductivity values on defibrillation thresholds in a simple heart-in-a-bath model. A generalised polynomial chaos approach is used to generate 41 sets of four cardiac conductivity values based on the three commonly used data sets. Simulations, using the bidomain equations, are performed on an isolated heart placed in a bath with a pair of defibrillation paddles, of varying potential differences, at the sides of the bath. The polynomial chaos approach allows the calculation of mean and variance of extracellular potential and potential gradient fields within the heart. The results show that conductivity values have a significant effect on the thresholds required to defibrillate the heart.

1. Introduction

It has been known for some time that the values for conductivity used in bidomain models of cardiac tissue lead to significant differences in the epicardial potential distributions that arise from subendocardial ischaemia during the ST segment [1, 2]. These studies show that for a given shape and thickness of the ischaemic region, the resulting epicardial potential distributions can show anything from ST elevation over the boarders of the ischaemic region (using the data of Clerc [3] or Roberts *et al.* [4]) to purely ST depression (using the data of Roberts and Scher [5]). These observations lead to questions of whether similar issues arise in models of other electrocardiographic scenarios. Here, the question of the effects of the above conductivity values on defibrillation thresholds will be examined.

Defibrillation is an important clinical tool in restoring the heart to normal sinus rhythm after some form of ventricular fibrillation. Restoration to sinus rhythm can be achieved by either external defibrillators or by an implanted cardioverter-defibrillator (ICD) [6]. While the correct application of potential differences across the heart via external defibrillators can be found via trial and error (as seen on many television programmes), it is much more critical for an ICD to achieve the correct potential difference the first time.

Consequently, accurate values for the conductivities are required in order to optimise the design of an ICD. Applying the correct potential difference to the heart the first time can increase the longevity of the ICD and not subject the patient to an unnecessarily large shock to restore sinus rhythm.

This study considers the simple situation of a heart in a bath. Generalised polynomial chaos is used to generate a range of conductivity values. These are then used in a bidomain model of the ventricles to determine the mean and variance of the extracellular potential distribution and the extracellular potential gradient for a given potential difference across the "paddles" in the model.

2. Methods

The simulation model for this study is a simple heart in a bath. The heart geometry was obtained from the Scientific Computing and Imaging Institute at the University of Utah and this has been used in previous studies of this nature [7]. For the simulations presented here, the heart is placed in a bath of fluid (equivalent to blood) which surrounds the heart and fills the ventricles (see Figure 1).

It is assumed that the equations governing the electric field in the heart are the passive bidomain equations [8, 9]

$$\nabla \cdot \mathbf{M_i} \nabla \phi_\mathbf{i} = -\mathbf{I_m} \quad \text{and} \quad \nabla \cdot \mathbf{M_e} \nabla \phi_\mathbf{e} = \mathbf{I_m} \tag{1}$$

where ϕ_h ($h = i$ or e) is the potential, (i=intracellular, e=extracellular), $\mathbf{M_h}$ are the conductivity tensors and I_m is the transmembrane current per unit volume. In general, the conductivity tensors can be written as

$$\mathbf{M_h} = \mathbf{A}\mathbf{G_h}\mathbf{A^T} \tag{2}$$

where $\mathbf{A}$ represents the local direction of the fibres and $\mathbf{G_h}$ is a diagonal matrix, containing the longitudinal (g_{hl}) and transverse (g_{ht}) tissue conductivities along the diagonal. It is further assumed that the conductivity normal to the tissue sheets is the same as the transverse conductivity. The electrical potential within the fluid, ϕ_b, is governed by Laplace's equation

$$\nabla^2 \phi_b = 0. \tag{3}$$

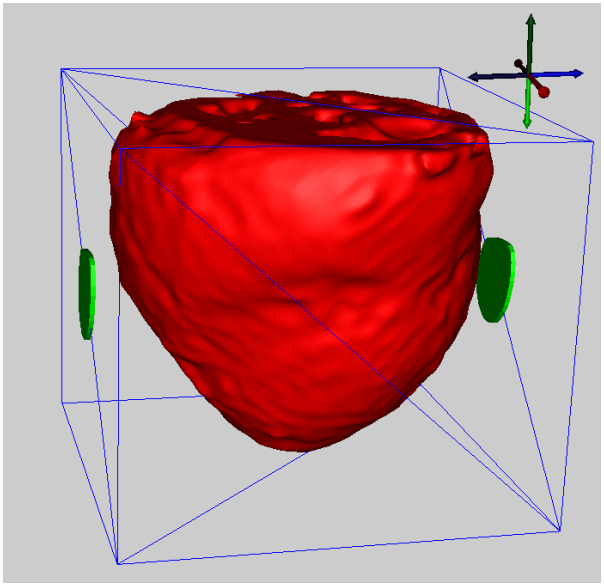

Figure 1. Model of the heart in a bath. The blue lines represent the outside of the bath and the green discs represent the defibrillation paddles.

For this simple model, the boundary conditions are that the surrounding bath is insulated, except for the region defined by the defibrillation paddles, where one paddle was maintained at 0V and the potential at other varied to create different potential differences across the heart. At the tissue–blood interfaces it is assumed that there is continuity of potential and current between the extracellular space and the blood. It is also assumed that the intracelllular space is insulated. In other words,

$$\phi_e = \phi_b, \quad g_{et}\frac{\partial \phi_e}{\partial n} = g_b \frac{\partial \phi_b}{\partial n}, \quad \frac{\partial \phi_i}{\partial n} = 0 \tag{4}$$

where $g_b = 0.67$mS/mm, is the conductivity of blood [10] and n is the outward pointing normal direction.

The governing equations (1) and (3), subject to the boundary and interface conditions (4), are solved using the finite element method as implemented in SCIRun [11]. An additional SCIRun module has been developed to compute the mass matrix for the finite element method.

The conductivity values obtained from various experiments are shown in Table 1, along with the respective extreme values. In order to apply generalised polynomial chaos on the conductivity values, some form of distribution for these values must be assumed. Given that there are only three data sets available, it is assumed that each conductivity value could be taken from a uniform distribution varying between the respective minimum and maximum.

Generalised polynomial chaos is a method of quantifying the uncertainty in the output from a mathematical model, given uncertainty in the input parameters [12]. In these simulations, the output is the electrical potential in the extracellular tissue and the input is the conductivity parameters. The generalised polynomial chaos is implemented via stochastic collocation [13, 14], where the collocation points are based on a Clenshaw-Curtis numerical integration scheme. Finally, Smolyak's method [15] is utilised to reduce the size of the integration space. Hence, having four conductivity values (i.e. four dimensions) and using third order integration results in 41 four dimensional integration points and 41 integration weights $w_j, \quad j = 1, \ldots, 41$. The 41 integration points are used to create 41 sets of four conductivities $(g_{il}^{(j)}, g_{it}^{(j)}, g_{el}^{(j)}, g_{et}^{(j)}), \quad j = 1, \ldots, 41$, by simple linear interpolation between the extremes on each conductivity value.

Table 1. Conductivity data (in mS/mm) from the indicated studies. Here the normal conductivities are taken to be equal to the transverse conductivity values.

Study	g_{el}	g_{et}	g_{il}	g_{it}
Clerc [3]	0.63	0.24	0.17	0.019
Roberts et al. [4]	0.22	0.13	0.28	0.026
Roberts and Scher [5]	0.12	0.08	0.34	0.06
Minimum	0.12	0.08	0.17	0.019
Maximum	0.63	0.24	0.34	0.06

Next, the governing equations (1), (3) are solved for each of the 41 conductivity sets. If $\phi_e^{(j)} = \phi_e(g_{il}^{(j)}, g_{it}^{(j)}, g_{el}^{(j)}, g_{et}^{(j)}), j = 1, \ldots, 41$, is the resulting extracellular potential distribution resulting from the conductivity values $(g_{il}^{(j)}, g_{it}^{(j)}, g_{el}^{(j)}, g_{et}^{(j)}), \quad j = 1, \ldots, 41$, then the mean extracellular potential distribution is given by

$$\overline{\phi_e} = \sum_{j=1}^{41} w_j \phi_e^{(j)} \tag{5}$$

and the variance of the extracellular potential distribution is

$$(\phi_e)_{\text{var}} = \sum_{j=1}^{41} w_j (\phi_e^{(j)} - \overline{\phi_e})^2. \tag{6}$$

It is also possible to calculate the mean and variance of the extracellular potential gradient field as

$$\overline{\nabla \phi_e} = \sum_{j=1}^{41} w_j \nabla \phi_e^{(j)} \tag{7}$$

and

$$(\nabla \phi_e)_{\text{var}} = \sum_{j=1}^{41} w_j (\nabla \phi_e^{(j)} - \overline{\nabla \phi_e})^2. \tag{8}$$

Table 2. Number of conductivity data sets (out of a maximum of 41 sets) for which the defibrillation threshold of 0.6V/mm in 90% of the tissue volume is met, for various potential differences across the defibrillator paddles.

Defibrillator Potential Difference (V)	Number of Conductivity Data Sets
150	0
160	1
170	3
180	8
190	18
200	28
210	33
220	38
230	41

3. Results

The governing equations are solved, as described above, for each of the 41 conductivity sets and for a range of potential differences across defibrillator paddles. Mean and variance fields are calculated for both the extracellular potential and the gradient of the extracellular potential. The potential differences used range from 150V up to 230V.

Table 2 shows the number of cardiac conductivity sets that meet the defibrillation threshold of 0.6V/mm over 90% of the volume of the heart tissue [6] for a given potential difference across the defibrillator paddles. It can been seen that a potential difference of 160V is required before any conductivity data sets meet this threshold. Overall, a potential difference of 230V is required for all conductivity data sets to meet the threshold. This large range of potential differences, 70V, is quite considerable relative to the 230V potential difference required for all conductivity data sets to meet the minimum threshold.

Figure 2 shows the mean extracellular potential gradient field, from the 41 different conductivity data sets in three cutting planes through the heart, for defibrillator paddle potential differences of 150V (top) and 230V (bottom). The mesh shown in the top panel of this figure indicates the outline of the heart. For the 150V potential difference, the only high potential gradients are seen near the epicardial and endocardial surfaces of the heart tissue. It can also be seen from the figure that the regions of lowest potential gradient are deep within the tissue. Regions near the paddles also show high potential gradients. With a potential difference of 230V, most of the tissue achieves the required 0.6V/mm potential gradient. However, there are still regions towards the centre of the heart, near the ventricles, that have low potential gradients.

Figure 3 shows the variance in the gradient of extracellular potential fields generated from the 41 conductivity data sets with defibrillator paddle potential differences of 150V (top) and 230V (bottom). In both cases the greatest variance in the potential gradients is near the surfaces of the heart. There are quite large regions of high variance in potential gradient around the outside of the heart and smaller regions around the walls of the ventricles. Deeper inside the tissue itself, the variance is small.

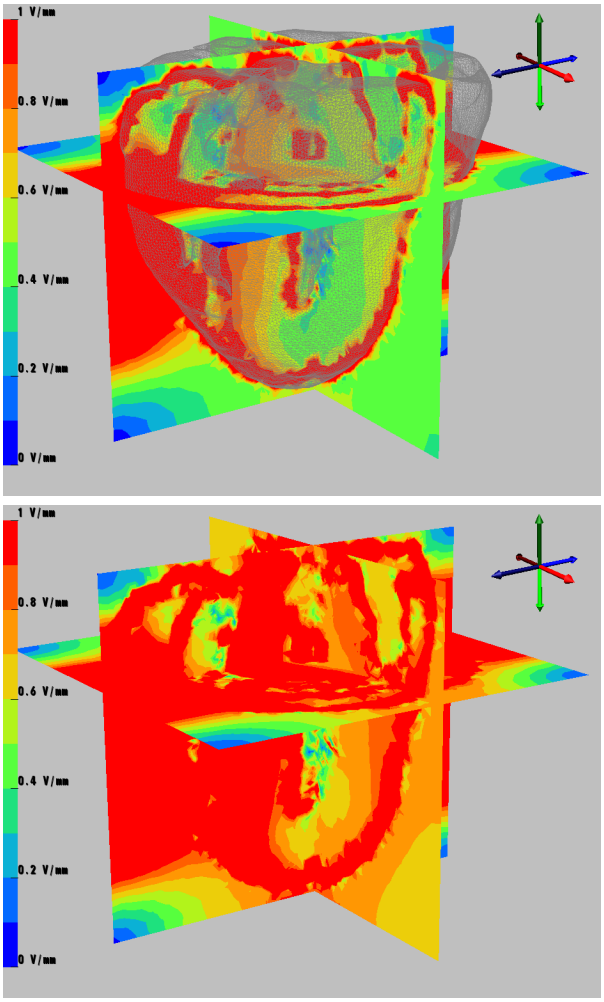

Figure 2. Average extracellular potential gradient field calculated from 41 sets of cardiac conductivity values for potential differences of 150V (top) and 230V (bottom) across the defibrillator paddles.

4. Conclusions

Conductivity values have a significant effect on the thresholds required to defibrillate the heart. In particular, there is up to a 70V difference between defibrillation thresholds depending on the conductivity values. Such a wide variation in the defibrillator paddle potential differ-

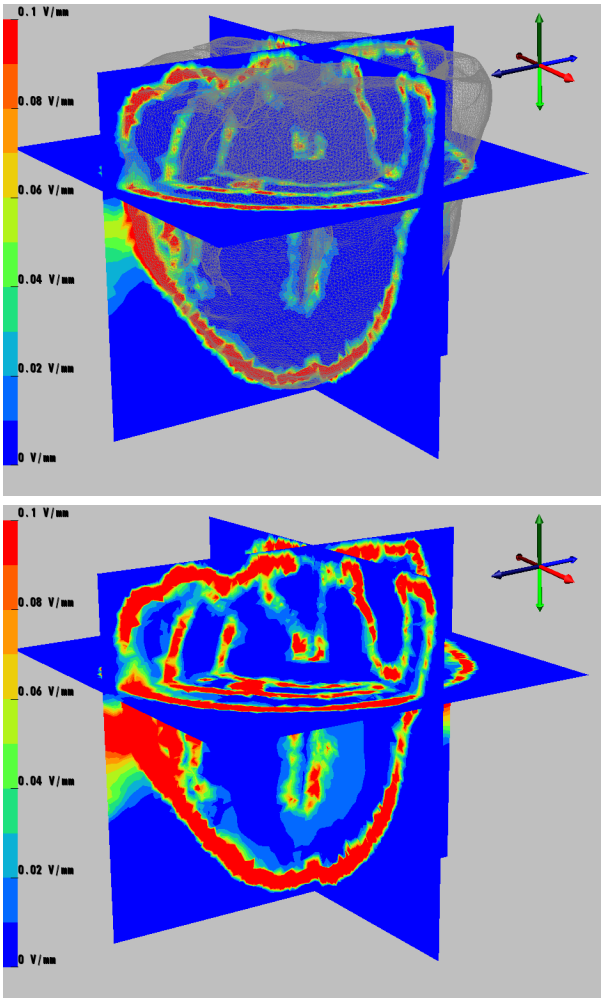

Figure 3. Variance of the extracellular potential gradient fields calculated from 41 sets of cardiac conductivity values for potential differences of 150V (top) and 230V (bottom) across the defibrillator paddles.

ence required to achieve the defibrillation threshold has the potential to impact on the design of ICDs. To obtain a more optimally designed ICD, a knowledge of more accurate cardiac conductivities would be a considerable advantage.

Acknowledgements

The author would like to thank Dr Jeroen Stinstra for writing the initial SCIRun mass matrix module and Prof Rob MacLeod for providing valuable discussions and insights during a sabbatical visit to the University of Utah in 2012.

References

[1] Johnston PR, Kilpatrick D, Li CY. The importance of anisotropy in modelling ST segment shift in subendocardial ischaemia. IEEE Transactions on Biomedical Engineering December 2001;48(12):1366–1376.

[2] Johnston PR, Kilpatrick D. The effect of conductivity values on ST segment shift in subendocardial ischaemia. IEEE Transactions on Biomedical Engineering February 2003; 50(2):150–158.

[3] Clerc L. Directional differences of impulse spread in trabecular muscle from mammalian heart. Journal of Physiology 1976;255:335–346.

[4] Roberts DE, Hersh LT, Scher AM. Influence of cardiac fiber orientation on wavefront voltage, conduction velocity and tissue resistivity in the dog. Circ Res 1979;44:701–712.

[5] Roberts DE, Scher AM. Effects of tissue anisotropy on extracellular potential fields in canine myocardium in situ. Circ Res 1982;50:342–351.

[6] Trayanova NA. Virtual 3d heart models to aid pacemaker implantation in children. Future Cardiology 2014/08/03/22:42:42 2013;10(1):5–8.

[7] Swenson D, Geneser S, Stinstra J, Kirby R, MacLeod R. Cardiac position sensitivity study in the electrocardiographic forward problem using stochastic collocation and boundary element methods. Annals of Biomedical Engineering 2012/10/27/15:28:04 2011;39(12):2900–2910.

[8] Arthur RM, Geselowitz DB. Effect of inhomogeneities on the apparent location and magnitude of a cardiac current dipole source. IEEE Trans Biomed Eng 1970;17:141–146.

[9] Tung L. A Bi–domain model for describing ischaemic myocardial D-C potentials. Ph.D. thesis, Massachusetts Institute of Technology, June 1978.

[10] Rush S, Abildskov JA, McFee R. Resistivity of body tissues at low frequencies. Circulation Research 1963;12:40–50.

[11] Sci institute, 2014. SCIRun: A Scientific Computing Problem Solving Environment, Scientific Computing and Imaging Institute (SCI), Download from: http://www.scirun.org.

[12] Xiu D, Em Karniadakis G. Modeling uncertainty in steady state diffusion problems via generalized polynomial chaos. Computer Methods in Applied Mechanics and Engineering 2012/10/29/23:39:58 2002;191(43):4927–4948.

[13] Xiu D, Hesthaven JS. High-order collocation methods for differential equations with random inputs. SIAM Journal on Scientific Computing 2013/08/08/04:30:58 2005; 27(3):1118–1139.

[14] Xiu D. Efficient collocational approach for parametric uncertainty analysis. Communications in Computational Physics 2007;2(2):293–309.

[15] Smolyak SA. Quadrature and interpolation formulas for tensor products of certain classes of function. Soviet Mathmeatics Doklady 1963;4:240–243.

Address for correspondence:

Peter Johnston, School of Natural Sciences, Griffith University
Nathan, Queensland, Australia, 4111, p.johnston@griffith.edu.au